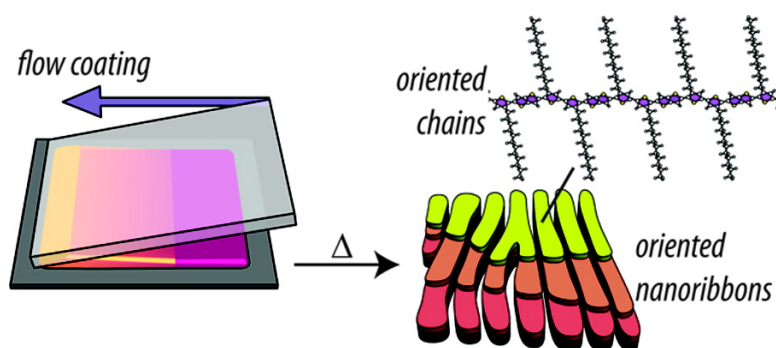


## Controlling the Orientation of Terraced Nanoscale “Ribbons” of a Poly(thiophene) Semiconductor

Dean M. DeLongchamp, R. Joseph Kline, Youngsuk Jung, David S. Germack, Eric K. Lin, Andrew J. Moad, Lee J. Richter, Michael F. Toney, Martin Heeney, and Iain McCulloch

ACS Nano, 2009, 3 (4), 780-787 • DOI: 10.1021/nn800574f • Publication Date (Web): 24 March 2009

Downloaded from <http://pubs.acs.org> on May 15, 2009



### More About This Article

Additional resources and features associated with this article are available within the HTML version:

- Supporting Information
- Access to high resolution figures
- Links to articles and content related to this article
- Copyright permission to reproduce figures and/or text from this article

[View the Full Text HTML](#)

# Controlling the Orientation of Terraced Nanoscale “Ribbons” of a Poly(thiophene) Semiconductor

Dean M. DeLongchamp,<sup>†,\*</sup> R. Joseph Kline,<sup>†</sup> Youngsuk Jung,<sup>†</sup> David S. Germack,<sup>†</sup> Eric K. Lin,<sup>†</sup> Andrew J. Moad,<sup>†</sup> Lee J. Richter,<sup>†</sup> Michael F. Toney,<sup>‡</sup> Martin Heeney,<sup>§</sup> and Iain McCulloch<sup>||</sup>

<sup>†</sup>National Institute of Standards and Technology, Gaithersburg, Maryland 20899, <sup>‡</sup>SSRL, <sup>§</sup>Queen Mary, University of London, London E1 4NS, U.K., and <sup>||</sup>Imperial College of London, London SW7 2AZ, U.K.

**ABSTRACT** The large-scale manufacture of organic electronics devices becomes more feasible if the molecular orientation and morphology of the semiconductor can be controlled. Here, we report on a previously unidentified crystal shape of terraced nanoscale “ribbons” in thin films of poly(2,5-bis(3-alkylthiophen-2-yl)thieno[3,2-*b*]thiophene) (pBTTT). The ribbons form after a pBTTT film is heated above its highest temperature phase transition. In contrast to the wide terrace crystal shape previously reported, terraced ribbons have lateral widths of  $\approx 60$  nm and lengths greater than 10  $\mu\text{m}$ , with a common orientation between adjacent ribbons. Further, we report a simple and scalable flow coating process that can control the ribbon orientation without requiring special substrates or external fields. The degree of molecular orientation is small after coating but increases dramatically after the terraced ribbons are formed, indicating that an oriented minority templates the whole film structure. The large extent of orientation obtained in these polythiophene crystallites provides potential opportunities to exploit anisotropic electrical properties and to obtain detailed information about the structure of organic semiconductor thin films.

**KEYWORDS:** polythiophene · crystal · nanoribbon · orientation · organic semiconductor

There is significant need to identify processing strategies to control the orientation of organic semiconductors because functional characteristics, such as charge carrier mobility<sup>1</sup> or the polarization of emitted light,<sup>2</sup> depend strongly on molecular and crystallographic orientation. Organic semiconductors with high carrier mobility are generally prepared as polycrystalline thin films with domains having a single common crystal contact plane parallel to the substrate but an isotropic distribution of the in-plane crystal axes. The molecules are therefore almost always oriented in the surface relative sense but lack the in-plane orientation control that would provide valuable opportunities to optimize device performance, tune material properties to specific applications, and enable novel device design. High levels of in-plane orientation can also greatly increase the amount of information that can be obtained from studies of organic semiconductor crystal

packing and microstructure formation,<sup>3</sup> making orientation control a potentially valuable element of characterization strategies.

An excellent candidate material for orientation control is the polymer semiconductor poly(2,5-bis(3-tetradecylthiophen-2-yl)thieno[3,2-*b*]thiophene) (pBTTT), which has exhibited high levels of order and field effect hole mobilities in transistors as high as  $1 \text{ cm}^2/\text{V} \cdot \text{s}$ .<sup>4–8</sup> The structure of pBTTT is shown in Figure 1. The high carrier mobility of pBTTT makes orientation control an attractive prospect because of the potential to maximize device properties. Furthermore, the packing structure of pBTTT may contain clues to its high performance, and oriented domains would greatly facilitate detailed structure analysis. Previous studies of pBTTT, however, have not revealed a tendency toward in-plane orientation. In this paper, we identify a previously unreported crystal form of pBTTT with a shape of nanoscale ribbons, which are formed after heating above the highest temperature phase transition. Because of their highly anisotropic shape, the terraced ribbons are a potentially ideal form in which to control the in-plane (azimuthal) orientation of pBTTT films.

In-plane (azimuthal) orientation control may be achieved by processing methods that align the in-plane crystallographic axes. This type of processing-induced orientation control is most often focused on liquid crystalline (LC) polymeric organic semi-

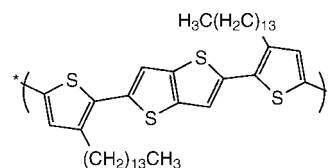


Figure 1. Molecular structure of pBTTT.

\*Address correspondence to dean.delongchamp@nist.gov.

Received for review September 12, 2008 and accepted March 11, 2009.

Published online March 24, 2009.  
10.1021/nn800574f CCC: \$40.75

© 2009 American Chemical Society

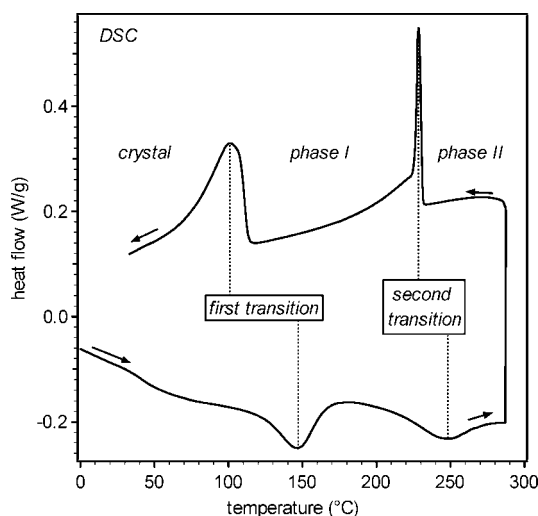


**Figure 2.** Second-scan DSC trace of pBTTT, exhibiting three phases.

conductors because the in-plane lattice usually includes the polymer backbone, which acts as a nematic mesogen. The alignment of the polymer backbone long axis with respect to confinement, shear, or other external fields is often exploited to achieve in-plane domain anisotropy. Orientation strategies applied to solid polymer semiconductors have included direct mechanical rubbing,<sup>9–13</sup> stretching<sup>14</sup> and shrinking,<sup>15</sup> friction transfer,<sup>16,17</sup> embossing,<sup>18</sup> and confinement.<sup>19</sup> Orientation strategies applied to melted, liquid crystalline, or solvated polymer semiconductors have included casting atop rubbed or grooved substrates,<sup>1,20–27</sup> directional solidification of a solvent,<sup>20,21</sup> and solidification within a magnetic field.<sup>28</sup>

Here, we describe a simple and scalable flow coating process that produces large films of well-oriented pBTTT terraced ribbons. With this process, high degrees of orientation can be achieved without the need for special substrates, external fields, or exotic treatments after casting; the orientation is induced by the coating process itself. The high extents of orientation in this system develop in a manner not previously reported for any polymer semiconductor: significant molecular orientation only occurs after a flow-coated film is heated into the polymer's highest temperature phase and then cooled. The large extent of orientation obtained may provide opportunities to exploit anisotropic electrical properties and to obtain detailed film structure information.

## RESULTS AND DISCUSSION

The polymer semiconductor pBTTT, shown in Figure 1, is a polythiophene derivative with a regiosymmetric monomer and linear alkane substitution. The pBTTT powder exhibits two distinct phase transitions in differential scanning calorimetry (DSC), as shown in Figure 2. We have recently shown that the first transition occurs by the melting of the alkane side chains,

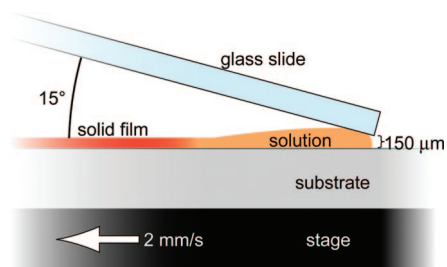


**Figure 3.** Flow-coating procedure used to control pBTTT orientation.

which are interdigitated and conformationally well-ordered in the room-temperature crystal.<sup>4</sup> The transition occurs at a similar temperature in thin films as it does in the powder measured by DSC. Heating films to the smectic-like<sup>4</sup> phase I enhances both film structure and field effect mobility by permitting the conjugated backbones to assume a more ideal vertical layer structure and allowing domains to grow in lateral size.<sup>5–7</sup> After a crystal  $\rightarrow$  phase I  $\rightarrow$  crystal thermal cycle, pBTTT films exhibit high levels of order in specular and grazing X-ray diffraction (XRD and GIXD), relatively large terraces of molecular height visible in atomic force microscopy (AFM), and excellent field effect hole mobilities.<sup>8</sup>

The DSC of pBTTT reveals that a second phase can be accessed at temperatures exceeding  $\sim 240$  °C (Figure 2). When pBTTT films were spin-coated atop hydrophobically modified silicon oxide dielectrics and then subjected to a crystal  $\rightarrow$  phase II  $\rightarrow$  crystal thermal cycle, we observed a loss of film cohesion (dewetting). In contrast, films spin-coated atop bare silicon oxide substrates and then thermally cycled exhibited a distinct surface topology of nanoscale terraced ribbons. The ribbons were found to orient concentrically about the center of the substrate, roughly perpendicular to the fluid flow direction during the spin-coating process. These results suggested that controlling the fluid flow direction with a unidirectional flow-coating process could produce uniformly oriented ribbons.

The flow-coating procedure used here is based on a method that uses a spreading blade and a translating stage, as shown in Figure 3. The flow-coating method was developed to provide combinatorial film thickness libraries for studying the thickness dependence of film dewetting,<sup>29</sup> crystallization,<sup>30</sup> and block copolymer ordering.<sup>31–33</sup> It has not been previously shown to induce molecular orientation. A pBTTT solution at 15 mg/mL in a 75 °C solvent mixture of 6:1 chloroform/dichlorobenzene (ratio by volume) was used for the coating process. Approximately 10  $\mu$ L of solution was syringed into a 150  $\mu$ m gap between the spreading blade, which was a clean glass slide, and the room-temperature substrate, which was a clean silicon wafer attached to the translating stage. The sample was then translated at a constant velocity of 2 mm/s so that the solution was spread evenly underneath the blade. This method differs from that previously

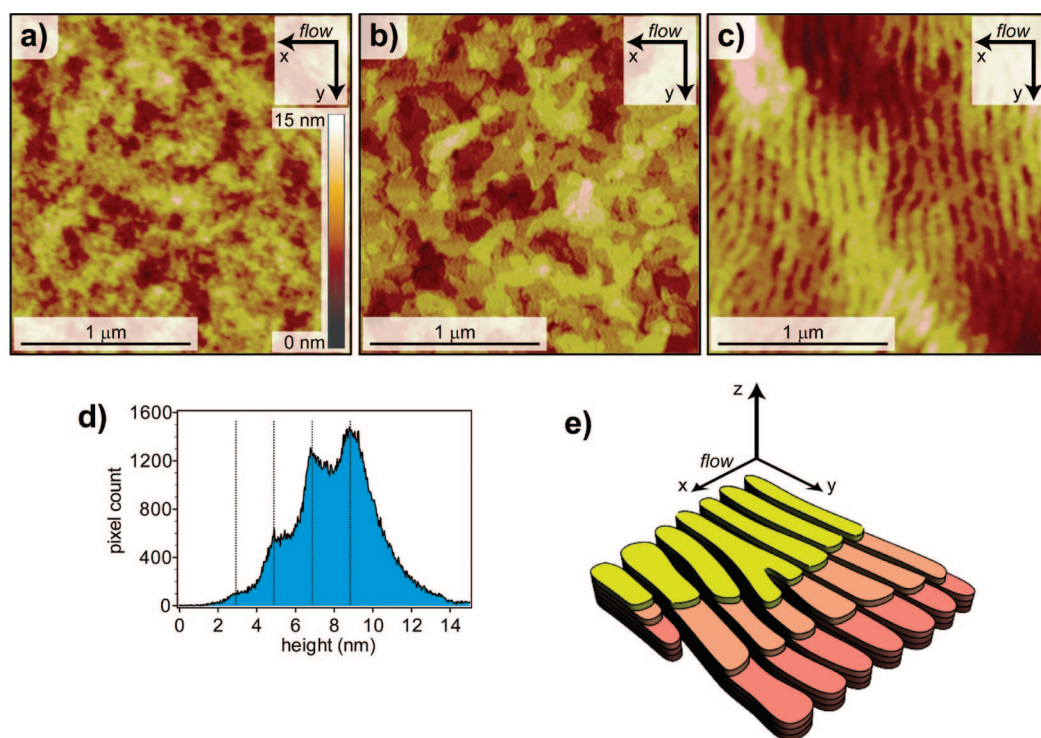


**Figure 4.** AFM images of flow-coated pBTTT films (a) after casting, (b) after thermal cycle to phase I exhibiting the wide terrace shape, and (c) after thermal cycle to phase II exhibiting the oriented ribbon shape. The direction of stage translation (flow) is marked on each image, and all images use the same color scale. (d) Height histogram of oriented ribbon image shown in panel c; (e) cartoon illustrating flow direction and ellipsometric axes with respect to ribbon direction.

reported<sup>29–33</sup> in that the table was translated in the same direction that the glass slide was tilted. A sharp transition region was observed underneath the glass slide with a width of  $\sim 1$  mm, where the solution became solid film. This region remained in a fixed position relative to the blade (e.g., the transition region moved at approximately the speed of the stage). The total translation distance was typically 5 cm, and the resultant films had typical lateral dimensions of  $2.5 \text{ cm} \times 5 \text{ cm}$ . The film thickness was  $\sim 30 \text{ nm}$  by spectroscopic ellipsometry (SE), the analysis and results of which we will describe in greater detail below. We note that it may be possible to fabricate films of arbitrarily large lateral dimensions by this method, provided that the blade and substrate can be made sufficiently parallel.

The flow-coated pBTTT films were studied by AFM to evaluate how well the process controlled the orientation of the surface topology. Flow-coated films with no thermal treatment, as shown in Figure 4a, exhibited relatively featureless surfaces with gradual height changes, similar to those we have previously reported for spin-coated and unheated pBTTT films.<sup>5</sup> Flow-coated films that were subjected to a crystal  $\rightarrow$  phase I  $\rightarrow$  crystal thermal cycle exhibited the terraced topology shown in Figure 4b, which is consistent with earlier reports for similarly heated spin-coated pBTTT films.<sup>5–7</sup> The terraces have lateral dimensions of  $100\text{--}500 \text{ nm}$  and a step height of  $\sim 2.1 \text{ nm}$  between terraces, consistent with each terrace being composed of a single mo-

lecular layer of pBTTT. Notably, no lateral orientation preference is observed in this terraced topology. We will hereafter refer to films cycled through phase I (up to  $180 \text{ }^\circ\text{C}$ ) as having a “wide terrace” micrometer-scale crystal shape.

Flow-coated films that were subjected to a crystal  $\rightarrow$  phase II  $\rightarrow$  crystal thermal cycle exhibit the distinct oriented ribbon topology shown in Figure 4c. The ribbons have varying lengths of  $1$  to  $>10 \text{ }\mu\text{m}$  and a width of roughly  $\sim 60 \text{ nm}$ . AFM indicates the presence of terraces on the ribbons. The terrace height can be determined using a height histogram, as shown in Figure 4d, which presents the distribution of pixel height in Figure 4c. The presence of four peaks in the histogram indicates four terrace levels, each with a uniform common height. The regular peak spacing of  $\sim 2.1 \text{ nm}$  reveals a terrace step height that corresponds to single molecular layers of pBTTT. The ribbon width of  $\sim 60 \text{ nm}$  corresponds to the expected end-to-end pBTTT backbone length for the  $\sim 28 \text{ kg/mol}$  number-average relative molecular mass used in this study. This correspondence suggests that the ribbon edges are polymer chain ends, and that the chains are perpendicular to the ribbon length. The uniform ribbon widths and terrace heights require that the ribbon interiors consist of pBTTT repeats lacking substantial *cis* rotations about the  $\text{sp}^2$  conjugated backbone. We will hereafter refer to films cycled through phase II (up to  $250 \text{ }^\circ\text{C}$ ) as having a “terraced ribbon” micrometer-scale crystal shape.

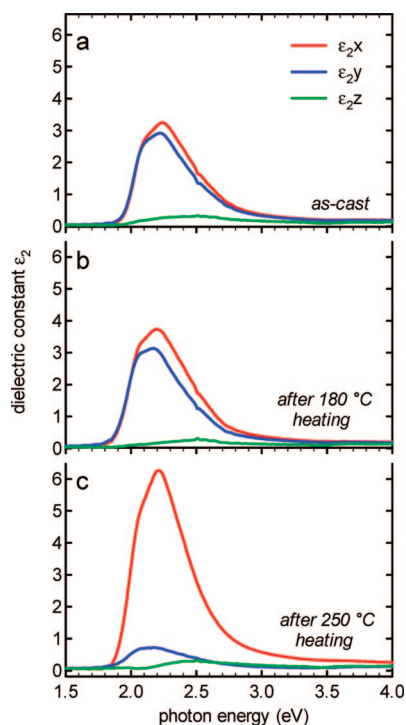


**Figure 5.** Imaginary parts of the dielectric function from spectroscopic ellipsometry of flow-coated films (a) after casting, (b) after cycled through phase I, and (c) after cycled through phase II. All data were collected at room temperature. Real parts of the dielectric function are available in Supporting Information.

The orientation of the pBTTT backbone can be determined from the biaxial dielectric function obtained through analysis of spectroscopic ellipsometry (SE) data collected from films oriented with the flow direction perpendicular and parallel to the incident beam. The separated imaginary components of the three-dimensional dielectric tensor are shown in Figure 5. The data are expressed as  $\epsilon_{2X}$ ,  $\epsilon_{2Y}$ , and  $\epsilon_{2Z}$  components, where the  $x$ -axis is parallel to the translation direction, and the  $z$ -axis is perpendicular to the substrate plane, as illustrated in Figure 4e. The most prominent feature common to all spectra is the peak at  $\sim 2.2$  eV (2.5 eV for the presumably disordered out-of-plane component), which corresponds to the backbone  $\pi-\pi^*$  transition. The transition dipole moment for this resonance lies parallel to the backbone long axis in thiophene polymers.<sup>34</sup> The relative intensities of the three imaginary components of the dielectric function therefore quantitatively describe the orientation of the pBTTT backbone with respect to the sample plane and flow-coating direction. In all three films, the in-plane backbone orientation ( $\epsilon_{2X} + \epsilon_{2Y}$ ) was far greater than the out-of-plane backbone orientation ( $\epsilon_{2Z}$ ), consistent with our previous measurements of spin-coated pBTTT films.<sup>6</sup> Flow-coated films of pBTTT without heat treatment exhibit only modest in-plane orientation ( $\epsilon_{2X}$  vs  $\epsilon_{2Y}$ ), as shown in Figure 5a. After the flow-coated films were cycled through phase I, the in-plane orientation increased somewhat but remained quite modest. Only

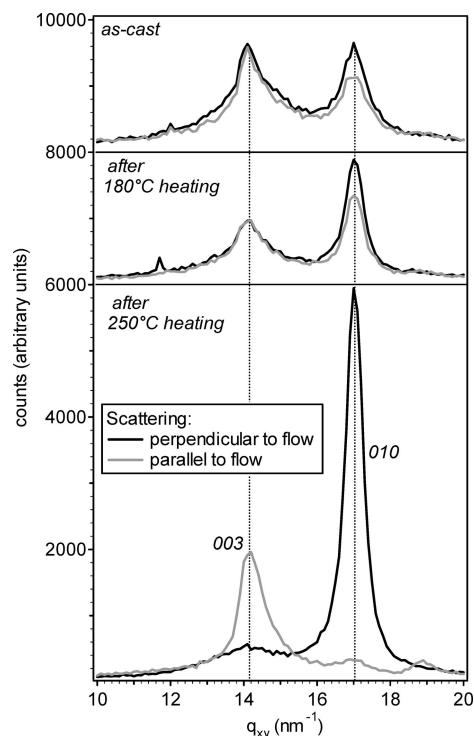


**Figure 6.** Grazing incidence X-ray diffraction of ribbon phase perpendicular and parallel to the flow direction.

after films were cycled through phase II was substantial in-plane orientation observed, as shown in Figure 5c. The pBTTT backbones within this film are oriented to a great extent along the flow direction. The backbones are therefore perpendicular to the ribbon length or parallel to the flow-coating direction, consistent with our conclusions from the AFM data.

Other important aspects of the pBTTT terraced ribbon phase are its crystalline quality and the orientation of its crystal unit cell. Specular XRD was employed to measure ordering along the surface normal (raw data shown in Supporting Information). The terraced ribbons exhibit 4 orders of ( $h00$ ) peaks indicating a layer–layer  $d$  spacing of  $\sim 2.05$  nm, consistent with the terrace height measured by AFM and similar to the spacing exhibited by the wide terraces. The peak widths are similar for all orders and, when analyzed by the Scherrer relationship ( $2\pi/[\text{full peak width at half-max}]$ ),<sup>35</sup> indicate a coherently ordered length that is equivalent to the film thickness, showing that the crystallites span the full film thickness.

The in-plane crystal orientation can be determined by GIXD, which measures the in-plane diffraction (unit cell dimensions, extent of orientation, and crystalline coherence). Films of pBTTT were measured in the GIXD geometry such that the scattering vector was oriented first perpendicular and then parallel to the flow direction. As shown in Figure 6, the GIXD patterns exhibit two prominent peaks, which we index using the orthorhombic cell suggested in ref 7. The (010) peak, with a spacing of 0.372 nm, corresponds to the  $\pi$ -stacking be-

tween laterally adjacent backbones. The (003) peak, with a repeat unit spacing of 1.33 nm, corresponds to the backbone long axis. For all films, the peak locations are identical within experimental error. Before proceeding with orientation analysis, we note that our results do not prove that the *b* and *c* lattice vectors are orthogonal. Given the observed systematic changes in peak intensity with sample rotation, however, the angle between them is likely close to 90°.

For pBTTT films that were not heated, or those cycled through phase I, the peak intensity varies little with scattering vector orientation. However, for films cycled through phase II, the results are dependent on sample orientation, as shown in Figure 6. When the scattering vector is parallel to the *y*-axis (perpendicular to the flow direction, as shown in Figure 4e), the (010) peak is prominent, whereas when the scattering vector is parallel to the *x*-axis, the (003) peak is prominent. This result shows that the  $\pi$ -stacking direction is oriented perpendicular to the flow direction, or along the ribbon length, and the backbones are oriented along the flow direction. These results agree well with the AFM and SE measurements of orientation. We note that when the Scherrer equation is applied to the in-plane diffraction peaks it delivers a coherence length of  $\sim 7$  nm, far smaller than the apparent terraced ribbon lateral dimensions. The in-plane diffraction peaks are likely broadened by defects within the domains, but a full defect analysis requires multiple peak orders, which typically are not observed.

At first glance, the very high extents of molecule and crystal orientation observed in the SE and X-ray diffraction of the terraced ribbons appear at odds with the defective and “wavy” appearance of the AFM images. Consideration of the specifics of ribbon packing, however, can reconcile the two observations. The edges of the ribbons are most likely formed from the ends of polymer chains. Since the energetic cost of poor chain end alignment is relatively small compared to the packing energy of the entire crystal, it is not surprising that misalignment occurs. In fact, significant chain end misalignments are inevitable because the polydispersity index (PDI) of the pBTTT used in this study is  $\sim 2$ ; therefore, the distribution of pBTTT chain lengths is broad, making perfect end alignment impossible. Small extents of polymer chain end misalignment could result in a curved ribbon contour even if the molecular orientation was perfect, as illustrated in Figure 7. The defects and “wavy” appearance of the ribbons shown in Figure 4 therefore remain consistent with the high levels of molecular orientation revealed by SE in Figure 5 and GIXD in Figure 6. Packing defects (which we know are present from the short coherence length along the (010) direction) may also play a secondary role in the wavy ribbon structure.

The terraced ribbons of pBTTT resemble reported fibrillar crystal shapes of regioregular poly(3-

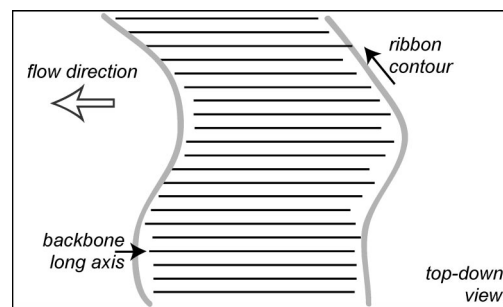


**Figure 7.** Cartoon showing one layer of a ribbon, demonstrating how slight misalignments of backbone long axes, even if they are perfectly oriented, could result in a curved ribbon contour.

hexylthiophene) (P3HT)<sup>36–39</sup> and some poly(fluorenes).<sup>40</sup> The general P3HT fibril organization, with  $\pi$ -stacking along the domain length and backbone orientation along the domain width, is quite similar to that of pBTTT ribbons. One notable difference, however, is that no terraces of molecular height have been reported for P3HT fibrils. Furthermore, the P3HT fibril width does not typically correlate with the molecular length. This effect is especially notable in molecular weight studies which show that the P3HT fibril width fails to increase for number-average molecular mass greater than  $\sim 7$  kg/mol.<sup>38,41</sup> The maximum P3HT fibril width appears to be  $\sim 30$  nm,<sup>38,41</sup> smaller than the  $\sim 60$  nm of pBTTT ribbons (which corresponds to a fully extended chain). This comparison suggests that terraced ribbon is a potential crystal shape for all thiophene polymers, but its realization in P3HT (and possibly other thiophene derivatives) is frustrated by packing defects or backbone torsion. It is also possible that differences in room-temperature side chain character are the root cause of these differences; pBTTT has crystalline, interdigitated side chains, whereas P3HT has liquid-like, noninterdigitated side chains.<sup>42</sup> The side chains of P3HT provide no mechanism for registry of vertically adjacent layers, which may explain the lack of terraces in P3HT fibrils.

The diffraction results indicate that the spacings of the primary crystal planes,  $d_{003}$ ,  $d_{010}$ , and  $d_{100}$ , are the same, within error, for the terraced ribbons and wide terraces. However, without lattice angle information, we cannot prove that the unit cells are identical. Nonetheless, this observed similarity suggests that the terraced ribbons are simply a form of the wide terraces with aligned chain ends and uniformly oriented backbones. In wide terraces, every lateral dimension is typically wider than the  $\sim 60$  nm length of a single pBTTT chain, so a number of chain ends must reside inside the layers. Laterally adjacent chain ends within the domains would be a packing defect that would interrupt regular ordering along the [001] lattice direction. In the terraced ribbons, the interior chain ends are presumably pushed outward to the grain boundaries, eliminating this packing defect.

Since terraced ribbons only occur after cycling to phase II, the freedom of molecular motion is presumably greater within phase II than within phase I. The lack of significant orientation upon heating to phase I, where the solvent should be evaporated, suggests that the solvent plays a minimal role in the rearrangement and phase behavior that occurs in phase II. We have previously studied phase I and classified it as a high-order smectic mesophase, with layered backbones and well-defined  $\pi$ -stacking between backbone planes, but having liquid side chains and presumably lacking registry between vertically adjacent layers.<sup>4</sup> We hypothesize that, because  $\pi$ -stacking is maintained in phase I, the lateral translation of the backbones is highly constrained and therefore ribbons cannot form. As the chain ends are moved to the domain edges after entering phase II, this constraint appears relaxed, which strongly suggests that  $\pi$ -stacking is disrupted in phase II. A low viscosity, liquid-like phase II was suggested by the dewetting that occurred in films cast atop hydrophobic substrates. The comprehensive in-plane reorientation of the backbones to conform to a minority of molecules is further evidence of significant backbone freedom. The phase I  $\rightarrow$  phase II transition may therefore be tentatively regarded as backbone melting.

Many polymer semiconductor orientation strategies have exploited the nematic character of other so-called “hairy rod” polymers with rigid backbones and alkane side chain substitution. Most notably, the nematic phases of the polyfluorenes (PFs, both pure and copolymerized with thiophene) have been widely exploited to achieve in-plane backbone alignment,<sup>3,40,43</sup> albeit not by flow-coating techniques. The alignment of PF backbones has been used to study anisotropy in carrier mobility<sup>1</sup> and electroluminescence.<sup>2</sup> We note that the alignment of pBTTT backbones in phase II may appear to resemble the orientational behavior of nematic PFs, which would suggest that phase II is of nematic character. Our preliminary analysis, however, suggests that phase II is not nematic. Birefringence under cross-polarized optical microscopy is eliminated by *in situ* heating to phase II, suggesting that most of the pBTTT backbones do not have in-plane orientation within this phase. Preliminary SE with *in situ* heating to  $\sim 240$  °C indicates that phase II exhibits little out-of-plane anisotropy and pronounced thermochromism (compared to phase I), consistent with significant torsional disorder along the chain. These considerations suggest that phase II is far less ordered than a typical nematic system.

The original orientation created by the flow coating represents a minority component of the molecules within the film, as evidenced by the AFM, SE, and diffraction data. The mechanism by which this minority component seeds orientation after entering phase II is currently unclear. However, two hypotheses could explain the initial development of the “seed” orientation. Our first hypothesis is that the orientation is caused by shear, which would arise from the narrow gap, the velocity of vertical translation, and the relatively high viscosity of the polymer solution. This hypothesis would require that the pBTTT in solution adopt a lyotropic (solvent-dependent) nematic state. Our second hypothesis is that the orientation is caused by the fixed propagation direction of film drying. This second hypothesis could be considered directional crystallization, albeit not of a solid solvent as has been used in other studies,<sup>20,21</sup> but of the polymer itself. For example, orientation control has been observed in some paraffins where the chain axis becomes parallel to the solidification direction under directional solidification from a melt.<sup>44,45</sup> Discrimination between these two hypotheses presents a significant challenge.

## CONCLUSIONS

We have shown that a previously unreported terraced ribbon crystal shape of pBTTT can be formed after heating above its highest temperature phase transition. The orientation of the terraced pBTTT ribbons can be controlled with a simple flow-coating method. The high levels of orientation that can be achieved provide opportunities to study or exploit the anisotropy of the functional properties of the polymer semiconductor. For example, we are currently assessing strategies to study anisotropy in charge carrier mobility. One complicating factor is that the terraced ribbons can only be formed on substrates upon which the film remains cohesive in phase II, which does not permit the important hydrophobic dielectric modification typically required for high performance in bottom-gated organic transistors. We also speculate that this technique will orient other thiophene polymers. Promisingly, most thiophene polymers with a number-average relative molecular mass greater than  $\sim 10$  kg/mol exhibit a backbone melting transition between 220 and 270 °C. The flow-coating method could become a valuable means to compare and control polymer semiconductor structure and function.

## MATERIALS AND METHODS

**Materials.** The polymer semiconductor pBTTT was synthesized by Stille coupling according to previously described methods.<sup>5,46</sup> The number-average molecular mass was found by gel permeation chromatography with chlorobenzene to be  $\sim 28$  kg/mol. Differential scanning calorimetry (DSC) measure-

ments were performed on pBTTT powder using a TA-Q1000<sup>47</sup> with a heating and cooling rate of 10 °C/min. The pBTTT was dissolved at a concentration 15 mg/mL in a solvent mixture of 6:1 chloroform/1,2-dichlorobenzene at  $\sim 70$  °C in a valve-sealed, pressure-resistant vial (Mini-inert; Supelco). Substrates were (100) silicon wafers cleaned by 10 min exposure to ultraviolet-

generated ozone (UVO, Jelight Model 42). Flow-coating blades were 25 mm × 75 mm glass microscope slides (Corning) also cleaned by 10 min exposure to UVO.

**Film Preparation.** Films were prepared using the flow-coating technique, which has been previously described.<sup>29–33</sup> The substrate was temporarily adhered to a custom-built, motorized translation stage. Approximately 15  $\mu\text{L}$  of the pBTTT solution was dispensed from a warmed syringe into the gap under the stationary knife blade fixed at 150  $\mu\text{m}$  above the substrate surface. The solution rapidly filled the gap. The substrate was not heated, so the solution cooled rapidly, and its color was observed to change from translucent orange to opaque maroon after dispensing. The stage was then immediately translated at 2 mm/s in the direction of blade tilt (note that it is translated away from the direction of blade tilt in the implementation described in previous work). Once the film appeared dry, the substrate was removed from the stage. Films were thermally cycled through phase I by placement on an aluminum hot plate held at 180 °C for 10 min, after which the hot plate and sample were allowed to cool to 80 °C in the ambient, which required  $\sim$ 30 min. Films were thermally cycled through phase II by placement on hot plate held at 250 °C for 10 min, with subsequent ambient cooling to 80 °C.

**Characterization.** AFM was performed on a Digital Instruments Nanoscope IV in tapping mode. Generalized spectroscopic ellipsometry (measurement of the off-diagonal elements of the Jones matrix) was collected at three angles from the surface plane (45, 27.5, and 10°) and four azimuthal angles from the flow direction (−45, 0, 45, and 90°) with an M 2000 series ellipsometer (J.A. Woollam Co., Inc.) and analyzed using vendor supplied software. To reduce correlations in the extracted uniaxial dielectric functions, measurements were made on identical films on two substrates: Si wafers terminated with native oxide or 200 nm thick thermal oxide. Specular XRD was performed on a Rigaku diffractometer with a Cu K $\alpha$  source. Grazing incidence X-ray diffraction (GIXD) was performed at the Stanford Synchrotron Radiation Laboratory on beamline 7-2; the films were illuminated with an 8 keV beam at a constant incidence angle of  $\sim$ 0.2°. The diffracted beam resolution was set by 1 mrad Soller slits.

**Acknowledgment.** Portions of this research were carried out at the Stanford Synchrotron Radiation Laboratory, a national user facility operated by Stanford University on behalf of the U.S. Department of Energy, Office of Basic Energy Sciences. The authors thank Dr. C. L. Soles for useful discussions.

**Supporting Information Available:** Specular XRD of pBTTT films. Real parts of the pBTTT dielectric function. This material is available free of charge via the Internet at <http://pubs.acs.org>.

## REFERENCES AND NOTES

- Sirringhaus, H.; Wilson, R. J.; Friend, R. H.; Inbasekaran, M.; Wu, W.; Woo, E. P.; Grell, M.; Bradley, D. D. C. Mobility Enhancement in Conjugated Polymer Field-Effect Transistors through Chain Alignment in a Liquid-Crystalline Phase. *Appl. Phys. Lett.* **2000**, *77*, 406–408.
- Grell, M.; Knoll, W.; Lupo, D.; Meisel, A.; Miteva, T.; Neher, D.; Nothofer, H. G.; Scherf, U.; Yasuda, A. Blue Polarized Electroluminescence from a Liquid Crystalline Polyfluorene. *Adv. Mater.* **1999**, *11*, 671–675.
- Knaapila, M.; Lyons, B. P.; Hase, T. P. A.; Pearson, C.; Petty, M. C.; Bouchenoire, L.; Thompson, P.; Serimaa, R.; Torkkeli, M.; Monkman, A. P. Influence of Molecular Weight on the Surface Morphology of Aligned, Branched Side-Chain Polyfluorene. *Adv. Funct. Mater.* **2005**, *15*, 1517–1522.
- DeLongchamp, D. M.; Kline, R. J.; Jung, Y.; Lin, E. K.; Fischer, D. A.; Gundlach, D. J.; Cotts, S. K.; Moad, A. J.; Richter, L. J.; Toney, M. F.; Heeney, M.; McCulloch, I. Molecular Basis of Mesophase Ordering in a Thiophene-Based Copolymer. *Macromolecules* **2008**, *41*, 5709–5715.
- McCulloch, I.; Heeney, M.; Bailey, C.; Genevicius, K.; Macdonald, I.; Shkunov, M.; Sparrowe, D.; Tierney, S.; Wagner, R.; Zhang, W. M.; Chabiny, M. L.; Kline, R. J.; McGehee, M. D.; Toney, M. F. Liquid-Crystalline Semiconducting Polymers with High Charge-Carrier Mobility. *Nat. Mater.* **2006**, *5*, 328–333.
- DeLongchamp, D. M.; Kline, R. J.; Lin, E. K.; Fischer, D. A.; Richter, L. J.; Lucas, L. A.; Heeney, M.; McCulloch, I.; Northrup, J. E. High Carrier Mobility Polythiophene Thin Films: Structure Determination by Experiment and Theory. *Adv. Mater.* **2007**, *19*, 833–837.
- Chabiny, M. L.; Toney, M. F.; Kline, R. J.; McCulloch, I.; Heeney, M. X-ray Scattering Study of Thin Films of Poly(2,5-bis(3-alkylthiophen-2-yl)thieno[3,2-*b*]thiophene). *J. Am. Chem. Soc.* **2007**, *129*, 3226–3237.
- Hamadani, B. H.; Gundlach, D. J.; McCulloch, I.; Heeney, M. Undoped Polythiophene Field-Effect Transistors with Mobility of 1 cm<sup>2</sup> V<sup>−1</sup> s<sup>−1</sup>. *Appl. Phys. Lett.* **2007**, *91*, 243512-1–243512-3.
- Bolognesi, A.; Botta, C.; Martinelli, M. Oriented Poly(3-alkylthiophene) Films: Absorption, Photoluminescence and Electroluminescence Behaviour. *Synth. Met.* **2001**, *121*, 1279–1280.
- Bolognesi, A.; Botta, C.; Mercogliano, C.; Marinelli, M.; Porzio, W.; Angiolini, L.; Salatelli, E. Oriented Thin Films from Soluble Polythiophenes. *Polym. Adv. Technol.* **2003**, *14*, 537–543.
- Bolognesi, A.; Botta, C.; Mercogliano, C.; Porzio, W.; Jukes, P. C.; Geoghegan, M.; Grell, M.; Durell, M.; Trolley, D.; Das, A.; Macdonald, J. E. Structural Features in Aligned Poly(3-alkylthiophene) Films Revealed by Grazing Incidence X-ray Diffraction. *Polymer* **2004**, *45*, 4133–4138.
- Heil, H.; Finnberg, T.; von Malm, N.; Schmechel, R.; von Seggern, H. The Influence of Mechanical Rubbing on the Field-Effect Mobility in Polyhexylthiophene. *J. Appl. Phys.* **2003**, *93*, 1636–1641.
- Yang, C. Y.; Soci, C.; Moses, D.; Heeger, A. J. Aligned Rrp3ht Film: Structural Order and Transport Properties. *Synth. Met.* **2005**, *155*, 639–642.
- Dyreklev, P.; Inganas, O. Anisotropic DC-Conductivity in Stretch-Oriented Iodine-Doped Poly-3-(4-octylphenyl)-2,2'-bithiophene. *Synth. Met.* **1995**, *69*, 387–388.
- Backlund, T. G.; Sandberg, H. G. O.; Osterbacka, R.; Stubbs, H.; Torkkeli, M.; Serimaa, R. A Novel Method to Orient Semiconducting Polymer Films. *Adv. Funct. Mater.* **2005**, *15*, 1095–1099.
- Nagamatsu, S.; Tanigaki, N.; Yoshida, Y.; Takashima, W.; Yase, K.; Kaneto, K. Effects of Molecular Alignment on Carrier Transport in Organic Transistors. *Synth. Met.* **2003**, *137*, 923–924.
- Nagamatsu, S.; Takashima, W.; Kaneto, K.; Yoshida, Y.; Tanigaki, N.; Yase, K. Backbone Arrangement In “Friction-Transferred” Regioregular Poly(3-alkylthiophene)s. *Macromolecules* **2003**, *36*, 5252–5257.
- Hu, Z.; Muls, B.; Gence, L.; Serban, D. A.; Hofkens, J.; Melinte, S.; Nysten, B.; Demoustier-Champagne, S.; Jonas, A. M. High-Throughput Fabrication of Organic Nanowire Devices with Preferential Internal Alignment and Improved Performance. *Nano Lett.* **2007**, *7*, 3639–3644.
- Zheng, Z. J.; Yim, K. H.; Saifullah, M. S. M.; Welland, M. E.; Friend, R. H.; Kim, J. S.; Huck, W. T. S. Uniaxial Alignment of Liquid-Crystalline Conjugated Polymers by Nanoconfinement. *Nano Lett.* **2007**, *7*, 987–992.
- Brinkmann, M.; Rannou, P. Effect of Molecular Weight on the Structure and Morphology of Oriented Thin Films of Regioregular Poly(3-hexylthiophene) Grown by Directional Epitaxial Solidification. *Adv. Funct. Mater.* **2007**, *17*, 101–108.
- Brinkmann, M.; Wittmann, J. C. Orientation of Regioregular Poly(3-hexylthiophene) by Directional Solidification: A Simple Method to Reveal the Semicrystalline Structure of a Conjugated Polymer. *Adv. Mater.* **2006**, *18*, 860–863.
- Banach, M. J.; Friend, R. H.; Sirringhaus, H. Influence of the Molecular Weight on the Thermotropic Alignment of Thin Liquid Crystalline Polyfluorene Copolymer Films. *Macromolecules* **2003**, *36*, 2838–2844.
- Banach, M. J.; Friend, R. H.; Sirringhaus, H. Influence of the Casting Solvent on the Thermotropic Alignment of Thin

- Liquid Crystalline Polyfluorene Copolymer Films. *Macromolecules* **2004**, *37*, 6079–6085.
24. Fernandez-Blazquez, J. P.; Bello, A.; Perez, E. Parallel and Perpendicular Orientation in a Thermotropic Main-Chain Liquid-Crystalline Polymer. *Macromolecules* **2007**, *40*, 703–709.
  25. Pattison, L. R.; Hexemer, A.; Kramer, E. J.; Krishnan, S.; Petroff, P. M.; Fischer, D. A. Probing the Ordering of Semiconducting Fluorene-Thiophene Copolymer Surfaces on Rubbed Polyimide Substrates by Near-Edge X-ray Absorption Fine Structure. *Macromolecules* **2006**, *39*, 2225–2231.
  26. Knaapila, M.; Hase, T. P. A.; Torkkeli, M.; Stepanyan, R.; Bouchenoire, L.; Cheun, H.-S.; Winokur, M. J.; Monkman, A. P. Meridional Orientation in Biaxially Aligned Thin Films of Hairy-Rod Polyfluorene. *Cryst. Growth Des.* **2007**, *7*, 1706–1711.
  27. Amundson, K. R.; Sapjeta, B. J.; Lovinger, A. J.; Bao, Z. N. An In-Plane Anisotropic Organic Semiconductor Based Upon Poly(3-hexyl thiophene). *Thin Solid Films* **2002**, *414*, 143–149.
  28. Tao, Y. F.; Zohar, H.; Olsen, B. D.; Segalman, R. A. Hierarchical Nanostructure Control in Rod-Coil Block Copolymers with Magnetic Fields. *Nano Lett.* **2007**, *7*, 2742–2746.
  29. Meredith, J. C.; Smith, A. P.; Karim, A.; Amis, E. J. Combinatorial Materials Science for Polymer Thin-Film Dewetting. *Macromolecules* **2000**, *33*, 9747–9756.
  30. Beers, K. L.; Douglas, J. F.; Amis, E. J.; Karim, A. Combinatorial Measurements of Crystallization Growth Rate and Morphology in Thin Films of Isotactic Polystyrene. *Langmuir* **2003**, *19*, 3935–3940.
  31. Smith, A. P.; Douglas, J. F.; Meredith, J. C.; Amis, E. J.; Karim, A. High-Throughput Characterization of Pattern Formation in Symmetric Diblock Copolymer Films. *J. Polym. Sci., Part B: Polym. Phys.* **2001**, *39*, 2141–2158.
  32. Smith, A. P.; Sehgal, A.; Douglas, J. F.; Karim, A.; Amis, E. J. Combinatorial Mapping of Surface Energy Effects on Diblock Copolymer Thin Film Ordering. *Macromol. Rapid Commun.* **2003**, *24*, 131–135.
  33. Epps, T. H.; DeLongchamp, D. M.; Fasolka, M. J.; Fischer, D. A.; Jablonski, E. L. Substrate Surface Energy Dependent Morphology and Dewetting in an ABC Triblock Copolymer Film. *Langmuir* **2007**, *23*, 3355–3362.
  34. Erb, T.; Raleva, S.; Zhokhavets, U.; Gobsch, G.; Stuhn, B.; Spode, M.; Ambacher, O. Structural and Optical Properties of Both Pure Poly(3-octylthiophene) (P3OT) and P3OT/Fullerene Films. *Thin Solid Films* **2004**, *450*, 97–100.
  35. Scherrer, P. *Nachr. Göttinger Gesell.* **1918**, *98*, 394.
  36. Jeff Moulton, P. S. Gel Processing of Electrically Conductive Blends of Poly(3-Octylthiophene) and Ultrahigh Molecular Weight Polyethylene. *J. Polym. Sci., Part B: Polym. Phys.* **1992**, *30*, 871–878.
  37. Yang, H. C.; Shin, T. J.; Yang, L.; Cho, K.; Ryu, C. Y.; Bao, Z. N. Effect of Mesoscale Crystalline Structure on the Field-Effect Mobility of Regioregular Poly(3-hexyl thiophene) in Thin-Film Transistors. *Adv. Funct. Mater.* **2005**, *15*, 671–676.
  38. Zhang, R.; Li, B.; Iovu, M. C.; Jeffries-El, M.; Sauve, G.; Cooper, J.; Jia, S. J.; Tristram-Nagle, S.; Smilgies, D. M.; Lambeth, D. N.; McCullough, R. D.; Kowalewski, T. Nanostructure Dependence of Field-Effect Mobility in Regioregular Poly(3-hexylthiophene) Thin Film Field Effect Transistors. *J. Am. Chem. Soc.* **2006**, *128*, 3480–3481.
  39. Iovu, M. C.; Zhang, R.; Cooper, J. R.; Smilgies, D. M.; Javier, A. E.; Sheina, E. E.; Kowalewski, T.; McCullough, R. D. Conducting Block Copolymers of Regioregular Poly(3-hexylthiophene) and Poly(methacrylates): Electronic Materials with Variable Conductivities and Degrees of Interfibrillar Order. *Macromol. Rapid Commun.* **2007**, *28*, 1816–1824.
  40. Lieser, G.; Oda, M.; Miteva, T.; Meisel, A.; Nothofer, H. G.; Scherf, U.; Neher, D. Ordering, Graphoepitaxial Orientation, and Conformation of a Polyfluorene Derivative of The “Hairy-Rod” Type on an Oriented Substrate of Polyimide. *Macromolecules* **2000**, *33*, 4490–4495.
  41. Yang, H. C.; Shin, T. J.; Bao, Z. N.; Ryu, C. Y. Structural Transitions of Nanocrystalline Domains in Regioregular Poly(3-hexyl thiophene) Thin Films. *J. Polym. Sci., Part B: Polym. Phys.* **2007**, *45*, 1303–1312.
  42. Gurau, M. C.; Delongchamp, D. M.; Vogel, B. M.; Lin, E. K.; Fischer, D. A.; Sambasivan, S.; Richter, L. J. Measuring Molecular Order in Poly(3-alkylthiophene) Thin Films with Polarizing Spectroscopies. *Langmuir* **2007**, *23*, 834–842.
  43. Grell, M.; Bradley, D. D. C.; Inbasekaran, M.; Woo, E. P. A Glass-Forming Conjugated Main-Chain Liquid Crystal Polymer for Polarized Electroluminescence Applications. *Adv. Mater.* **1997**, *9*, 798–802.
  44. Asano, T. Melt-Crystallization of Normal-Alkanes and Polyethylene in a Temperature-Gradient 2. Melt-Orientation of Hexatriacontane (C<sub>36</sub>H<sub>74</sub>). *Polym. Bull.* **1984**, *12*, 543–546.
  45. Asano, T.; Mina, M. F.; Nishida, A.; Yoshida, S.; Fujiwara, Y. Crystallization of a Low Molecular Weight Polyethylene and Paraffins under a Temperature Gradient. *J. Macromol. Sci.* **2001**, *B40*, 355–367.
  46. Tierney, S.; Heeney, M.; McCulloch, I. Microwave-Assisted Synthesis of Polythiophenes via the Stille Coupling. *Synth. Met.* **2005**, *148*, 195–198.
  47. Certain commercial equipment, instruments, or materials are identified in this paper to foster understanding. Such identification does not imply recommendation or endorsement by the National Institute of Standards and Technology, nor does it imply that the materials or equipment identified are necessarily the best available for this purpose.